

An optimal three-dimensional focusing technique for micro-flow cytometers

Chien-Hsiung Tsai · Hui-Hsiung Hou · Lung-Ming Fu

Received: 11 January 2008 / Accepted: 17 March 2008 / Published online: 22 April 2008
© Springer-Verlag 2008

Abstract This study presents a novel three-dimensional (3-D) hydrodynamic focusing technique for micro-flow cytometers. In the proposed approach, the sample stream is initially compressed in the horizontal direction by two sheath flows such that it is constrained in the central region of the microchannel. The sample stream is then focused in the vertical direction by a second pair of sheath flows and subsequently passes over a micro-weir structure positioned directly beneath an optical detection system. The micro-channel configuration and operational parameters are optimized by performing a series of numerical simulations to examine the effects on the sample stream distribution of the vertical and horizontal focusing ratios, the entrance angle of the second set of sheath flow channels, and the width and depth of the second set of sheath flow channels. The results indicate that the horizontal and vertical sheath flows successfully constrain the sample stream within a narrow, well-defined region of the microchannel. Furthermore, the micro-weir structure results in the separation of the cells/particles in the vertical direction and ensures that they flow in a sequential fashion through the detection region of the microchannel and can therefore be reliably counted. It is shown that the 3-D focusing technique can achieve a focused sample stream width of between 6 and 15 μm given an appropriate value of the horizontal focusing

ratio. Thus, the viability of the microflow cytometer for the counting and detection of individual biological cells is confirmed.

Keywords Micro-flow cytometer · Three-dimensional hydrodynamic focusing · Micro-weir structure · Numerical simulations

1 Introduction

With the rapid advances made in micro-electro-mechanical systems (MEMS) technologies over the past decade, the realization of micro-total-analysis-systems (μTAS) and “lab-on-a-chip” (LoC) devices has now emerged as a viable proposition (Erickson 2005; Lacharme and Gijs 2006; Lee et al. 2006; Tůma et al. 2007; Wu et al. 2007). In μTAS and LoC devices, various microfluidic components are integrated serially on a microchip in order to facilitate the complete assay of a bio-material. Typically, such devices incorporate DNA concentrators (e.g. Bown and Meinhart 2006), DNA digestion systems (e.g. Fu and Lin 2007), polymerase chain reactors (e.g. Prakash and Kaler 2007; Chang et al. 2006), optofluidic integration in micro-systems (Hunt and Wilkinson 2008), dielectrophoretic cell collection and separation systems (Zou et al. 2006; Chen and Du 2007), capillary electrophoresis on-line detection systems (Lin et al. 2004a), micro-mixers (Huang et al. 2006; Chang and Yang 2007), and microfluidic chips combined micromagnetic for separation of living cells (Xia et al. 2006). Compared to their large-scale counterparts, microfluidic devices have many significant advantages, including a reduced sample and reagent consumption, an improved sensitivity, a more rapid response time, a lower power consumption, greater portability, lower fabrication

C.-H. Tsai
Department of Vehicle Engineering,
National Pingtung University of Science and Technology,
Pingtung 912, Taiwan

H.-H. Hou · L.-M. Fu (✉)
Department of Materials Engineering,
National Pingtung University of Science and Technology,
Pingtung 912, Taiwan
e-mail: loudyfu@mail.npust.edu.tw

and operating costs, and the potential for integration with other miniaturized devices.

Micro-flow cytometers are designed to measure various physicochemical characteristics of suspended cells and are used in a wide variety of biomedical and industrial applications, including clinical hematology diagnosis, bacteria analysis, and gene diagnosis. In traditional planar micro-flow cytometers, the sample stream is focused hydrodynamically in the horizontal direction by two high-flow-rate sheath flows. These flows not only force the sample stream to flow along the central region of the microchannel, but also compress its width and therefore cause the cells/particles within the sample to flow in a sequential fashion in the downstream direction. However, the microfluidic devices fabricated standard micro-fabricated only facilitates the two-dimensional hydrodynamic focusing in the device plane by horizontally compressing the central stream flow into a thin stream flow between two neighboring sheath flows. Consequently, they are unable to focus the sample flow in the vertical direction.

Many applications of two-dimensional (2-D) hydrodynamic and electrokinetic focusing techniques have been presented in recent years (Fu et al. 2003; Emmelkamp et al. 2004; Stiles et al. 2005; Xuan and Li 2005; Lee et al. 2006; Zhuang et al. 2006; Kohlheyer et al. 2008; Yang and Hsieh 2007). For example, Lee et al. (2001) proposed a novel micro-flow cytometer fabricated using PDMS in which the sample stream was constrained to a width of less than 10 μm by positioning the sample injection nozzle in the center of an outer nozzle supplying a sheath flow at a relatively higher flow rate. In a later study, Lee et al. (2003) presented a novel 2-D hydrodynamic focusing flow cytometer system with integrated optical waveguides. McClain et al. (2001, 2003) developed a 2-D electrokinetic focusing micro-flow cytometer for the detection of fluorescently labeled-*E. coli* bacteria. In the proposed device, the living cells were transported through the cytometer electrophoretically and were focused into a single-cell stream for detection purposes via buffer flows introduced through microchannels arranged perpendicularly to the main flow channel. The experimental results demonstrated that the majority of the cells survived the electric field used to effect their transport and could be successfully detected at throughput rates ranging from 30 to 85 cells/s. Rodriguez-Trujillo et al. (2007) presented a low-cost micro-Coulter counter fabricated from PMDS and glass and showed that the use of a tunable 2-D hydrodynamic focusing technique enabled the device to probe particles with a wide range of diameters. The performance of the device was demonstrated experimentally via the counting of latex micro-beads with a diameter of 20 μm . Fu et al. (2004a) developed a 2-D electrokinetic focusing micro-fluidic system with multiple side channels for the detection

and sorting of cells/particles of different diameters. In the proposed device, the cells/particles were detected using an optical fiber embedded in the microchip and coupled with a gas laser and an avalanche photodetector.

As described above, in traditional planar micro-cytometers, the sample stream is compressed via a 2-D focusing effect such that its width approaches that of the cell size. As a result, the cells within the sample stream are forced to flow sequentially through the detection region. However, since the hydrodynamic sheath flows focus the sample stream only in the horizontal direction, there is no guarantee that the cells do not overlap one another in the vertical direction. Furthermore, the detection systems used in typical micro-cytometers are unable to detect cells if their depths in the sample do not coincide with the focal plane of the observation lens. As a result, the use of a 2-D focusing technique inevitably limits the detection and counting performance of micro-flow cytometers. In an attempt to resolve this problem, researchers have proposed a variety of 3-D focusing techniques, including dielectrophoresis (DEP) force focusing (Yu et al. 2005; Holmes et al. 2006; Cheng et al. 2007), 2-D hydrodynamic focusing combined with a negative DEP force (Lin et al. 2004b; Wang et al. 2006) and 3-D hydrodynamic focusing (Wolff et al. 2003; Dittrich and Schwille 2003; Sundararajan et al. 2004; Yang et al. 2005; Mao et al. 2007; Chang et al. 2007). In the 3-D DEP force focusing technique presented by Cheng et al. (2007), the motion of the cells/particles in the channel is regulated by two forces, namely a hydrodynamic force in the streamwise direction and a negative DEP force in the cross-stream direction. This focusing technique has the advantage that sheath flows are not required, and thus the configuration of the cytometer is considerably more straightforward. Lin et al. (2004b) proposed a 3-D focusing micro-flow cytometer in which the sample stream was manipulated using a combination of a 2-D hydrodynamic focusing effect and a negative DEP force. In the proposed approach, two sheath flows were used initially to focus the sample flow horizontally and a negative DEP force generated by two embedded electrode plates was then used to focus the particles in the vertical direction. Dittrich and Schwille (2003) presented a 3-D hydrodynamic focusing micro-flow cytometer designed to enable the confocal detection of fluorescent cells/particles and to facilitate their sorting in accordance with their spectroscopic properties. The proposed cytometer featured a branched-channel configuration which not only enabled fluid mixing and a hydrodynamic focusing of the sample solution such that detection could be achieved, but also allowed the implementation of reaction steps prior to the detection and sorting processes. Mao et al. (2007) demonstrated a state-of-the-art fluid manipulation technique (utilizing sheath flow and

Dean vortices) to enable 3D hydrodynamic focusing with a simple single-layer planar microfluidic device fabricated via standard soft lithography.

The current study proposes a novel micro-flow cytometer in which the sample stream is focused three-dimensionally by two sets of sheath flows and a micro-weir structure. The basic configuration of the proposed device is illustrated in Fig. 1. As shown in Fig. 1a, the sample flow (i.e. the V_1 stream) is initially focused in the horizontal X - Y plane by the first pair of sheath flows (i.e. the V_2 streams) such that it is constrained to the central region of the microchannel. The sample stream is then focused in the vertical direction by the second pair of sheath flows (i.e. the V_3 streams) and subsequently passes over a micro-weir structure in the observation region of the channel (see Fig. 1c). The combined effect of the second pair of sheath flows and the micro-weir structure causes the individual cells/particles within the sample stream to separate in the vertical X - Z plane such that they flow through the observation region on a one-by-one basis and can therefore be individually counted. The cytometer configuration and the operational parameters are optimized by performing a series of computational fluid dynamics (CFD) simulations to examine the effects on the flow field within the cytometer of the vertical and horizontal focusing ratios, the entrance angle of the second set of sheath flow channels,

and the width and depth of the second set of sheath flow channels.

2 Numerical simulation procedures

Computational fluid dynamics (CFD) simulations enable the performance characteristics of cytometers (and all other forms of microfluidic device) to be extensively explored over a wide range of system parameters such that the optimal device design can be established before committing to the time and expense of fabricating actual physical models. In the CFD simulations, the flow field within the cytometer was modeled using the three-dimensional Navier–Stokes equation. Moreover, it was assumed that both the buffer flows and the sample stream were incompressible laminar flows with a negligible temperature variation. The governing conservation equations of mass, momentum and species are given respectively by

$$\frac{\partial U_j}{\partial x_j} = 0, \tag{1}$$

$$U_j \frac{\partial U_i}{\partial x_j} = -\frac{1}{\rho} \frac{\partial p}{\partial x_i} + \frac{\partial}{\partial x_j} \left(\nu \frac{\partial U_i}{\partial x_j} \right), \tag{2}$$

$$U_j \frac{\partial C}{\partial x_j} = D_C \frac{\partial}{\partial x_j} \left(\frac{\partial C}{\partial x_j} \right), \tag{3}$$

where U_i denotes the fluid velocity in the x_i direction, ρ is the density, ν is the kinematic viscosity, D_C is the binary diffusion coefficient, p is the static pressure and C is the species concentration. In the simulations, the values of ρ , ν and D_C were specified as $1,000 \text{ kg m}^{-3}$, 10^{-6} and $10^{-7} \text{ m}^2 \text{ s}^{-1}$, respectively. These values are the physical properties of the water and diluted dye-tinted water. Furthermore, the velocity and the species concentration at the flow inlet boundary was assumed to have a uniform profile, while a constant pressure and fully-developed conditions were imposed at the downstream boundary. Finally, no-slip conditions and an assumption of zero species concentration flux were applied at the solid walls of the cytometer.

The governing equations and their boundary conditions were solved numerically using the general purpose commercial CFD code FLUENT, which provides comprehensive modeling capabilities for a wide range of incompressible fluid flow problems. In the solution procedure, a finite-volume differencing scheme, a segregated solver, and an implicit technique were used to solve the algebraic equations formed by discretizing the closed set of governing equations. As recommended by Hardt and Schonfeld (2003), the spatial derivatives at all the interior grid points of the computational domain were approximated using a third-order QUICK scheme in order to minimize the effects of numerical diffusion (Tsai et al.

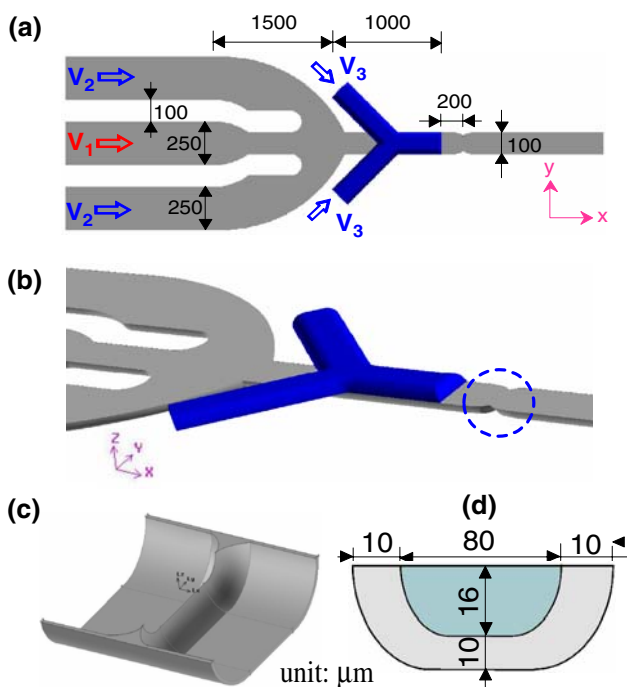


Fig. 1 a, b Schematic illustrations of micro-flow cytometer geometry seen from different directions, c 3D schematic of micro-weir structure, and d cross-section of micro-weir geometry

2007). Finally, the resulting difference equations for the pressure-velocity coupling in the Navier-Stokes equation were solved using the Semi-Implicit method for Pressure-Linked Equations (SIMPLE) algorithm (Van Doormal et al. 1984). Note that the under-relaxation technique was adopted to avoid divergence during the iterative solution procedure. To ensure a satisfactory resolution of the numerical results, the computational domain was discretized using structural hexahedral elements to construct a mesh containing approximately 800,000 cells. The code are verified using the experimental results for the horizontal focused stream width (Fu et al. 2008), the numerical results are concurred with the experimental results. The focused stream width is defined as the distance between the contours that have the constant species concentration of 0.8. Hence, the value is sensitive to the numerical diffusion. Since the QUICK third scheme is adopted and the grids numbers are large enough (800,000 cells), the numerical diffusion is minimized in the present study. Numerical experiments have been carried out to ensure that the focused width is grid independence.

3 Results and discussion

3.1 Effect of horizontal focusing ratio on stream width

In analyzing the focusing effect of the first sheath flow pair in the horizontal X - Y plane, the velocity of the sample flow (V_1) was fixed at 0.05 mm s and the sheath flow velocity (V_2) was varied from 0.05 to 0.3 mm s, resulting in a horizontal focusing ratio (V_2/V_1) ranging from 1:1 to 6:1. Figure 2 illustrates the numerical results obtained for the sample stream distribution within the flow cytometer for horizontal focusing ratios of 1:1, 3:1 and 5:1, respectively. It can be seen that the sheath flows compress the sample stream such that it flows along the central region of the microchannel. Furthermore, it is apparent that the sample stream retains an approximately constant focused width as it flows in the downstream direction.

Figure 3 illustrates the variation of the focused sample stream width in the horizontal X - Y plane as the horizontal focusing ratio is increased from 1:1 to 6:1. (Note that in computing the results, the focused stream width were measured at a cross-section located 2 mm downstream from the cytometer nozzle, i.e. immediately upstream of the micro-weir structure). It can be seen that the width of the focused sample stream decreases monotonically as the horizontal focusing ratio increases. The focused width does not strongly depend on the V_2/V_1 for $V_2/V_1 > 6$, the result is concurred with the experimental result of the paper (Fu et al. 2008). Individual biological cells, e.g. yeast cells, human red cells, human lung cancer cells, and so forth,

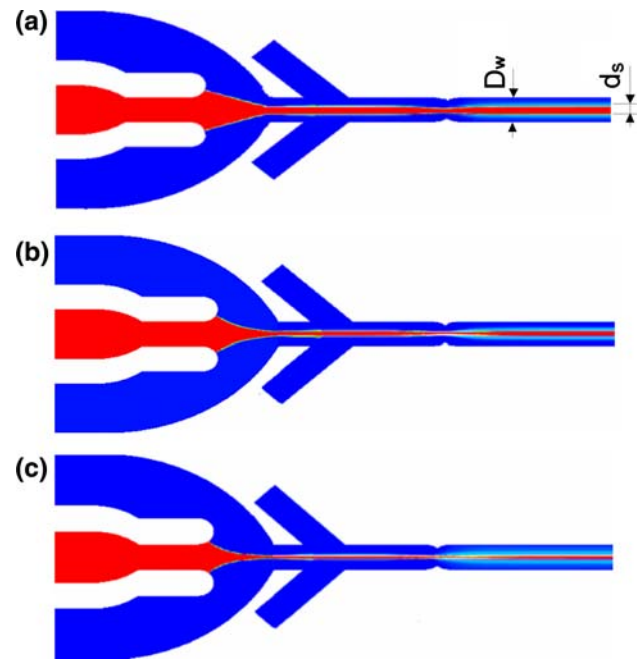


Fig. 2 Simulation results obtained for sample stream distribution under horizontal focusing ratios of: **a** 1:1, **b** 3:1 and **c** 5:1

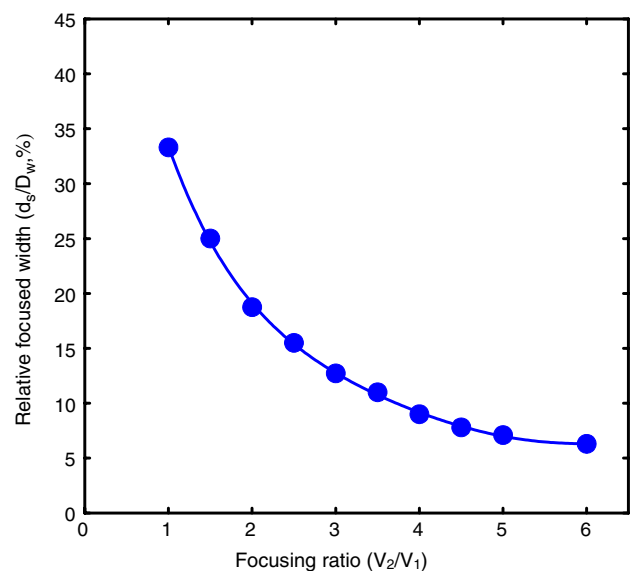


Fig. 3 Variation of focused stream width as function of horizontal focusing ratio

typically range from 5 to 15 μm in diameter. Therefore, in the present cytometer, the sample stream must be focused to a width of 15 μm (or less) to ensure that the cells pass through the observation region on a one-by-one basis in the horizontal X - Y plane. From Fig. 3, it can be seen that a horizontal focusing ratio of at least 2.5:1 is therefore required. The results suggest that the cytometer can be applied to detect cells with a diameter as small as 6 μm by specifying a horizontal focusing ratio of 6:1.

3.2 Respective effects of entrance angle of second sheath flow pair and vertical focusing ratio

A series of simulations was performed to investigate the effects of the entrance angle of the second sheath flow pair at various values of the vertical focusing ratio ($V_3:V_1$). In performing the simulations, the dimensions of the second set of sheath flow channels were assumed to be the same as those of the main microchannel of the cytometer, i.e. a width of 100 μm and a depth of 26 μm . Figure 4 presents the simulation results obtained for the cross-sectional distribution of the sample stream in the micro-weir region of the microchannel for entrance angles of 60°, 90° and 120°, respectively, and vertical focusing ratios of 1:1, 3:1, 5:1 and 7:1. Note that in every case, the horizontal focusing ratio was specified as 4:1 (corresponding to a stream width of $\sim 10 \mu\text{m}$, i.e. the mean width of typical biological cells). For the case of an entrance angle of 60°, it can be seen that a vertical focusing ratio of 7:1 yields a noticeable reduction in the focused height of the compressed sample stream. However, the results indicate that by increasing the entrance angle to 90° or 120°, respectively, a broadly similar reduction in the sample stream height can be obtained at a lower vertical focusing ratio of 5:1. The determination of the focused height h is the same as focused width.

Figure 5 illustrates the variation of the relative focused height of the compressed sample stream in the micro-weir region with the vertical focusing ratio (V_3/V_1) as a function of the entrance angle of the second set of sheath flow channels. As in Fig. 4, the horizontal focusing ratio is assumed to be 4:1 in every case. Note that the relative focused height is defined as: (height of focused sample stream h /height of microchannel in micro-weir region H) $\times 100\%$. The results show that when the vertical focusing ratio is assigned a low value, e.g. 1:1 \sim 3:1, the sample stream is reduced to around 60 \sim 70% of its original

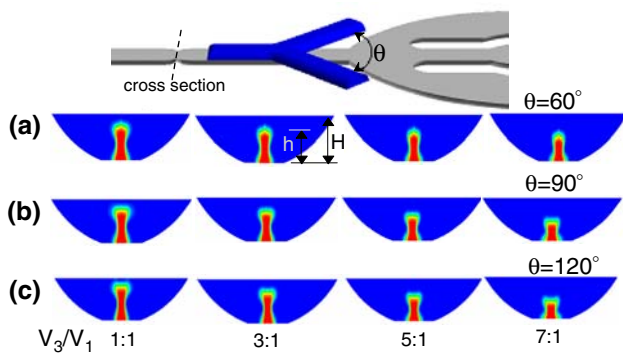


Fig. 4 Simulation results obtained for sample stream distribution in micro-weir region for a constant horizontal focusing ratio of 4:1, different vertical focusing ratios and secondary sheath flow angles of: **a** 60°, **b** 90° and **c** 120°

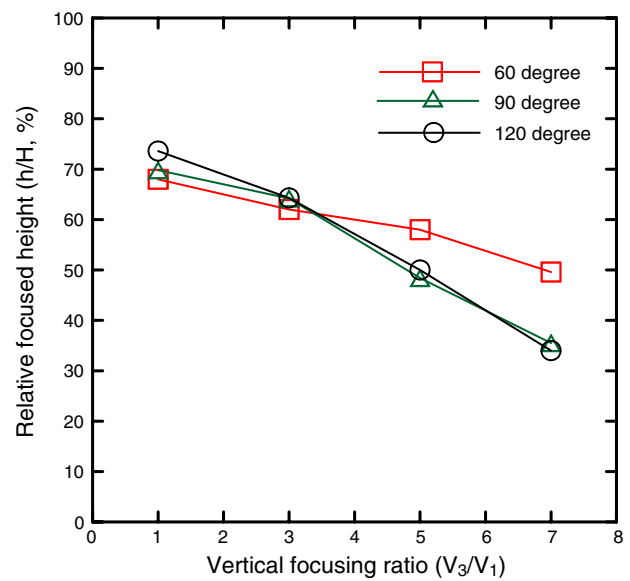


Fig. 5 Variation of relative focused height of sample stream in micro-weir region with vertical focusing ratio as function of secondary sheath flow angle. (Note that the results are obtained using a constant horizontal focusing ratio of 4:1.)

height irrespective of the entrance angle of the second sheath flow pair. However, as the vertical focusing ratio is increased, a further reduction in the height of the focused sample is obtained. It is apparent that the relative height of the sample is sensitive to the value of the entrance angle of the second set of sheath flow channels. For the lowest entrance angle of 60°, a less marked reduction in the sample height is obtained. However, at entrance angles of 90° and 120°, respectively, the relative sample height reduces rapidly as the vertical focusing ratio is increased. In general, a larger range of the relative focused height of the sample stream is indicative of a greater tuning ability and therefore enables a greater degree of control when performing cell detection and counting. Since no noticeable difference is observed, 90° is chosen arbitrarily to represent the optimal design for the second set of sheath flow channels.

3.3 Effect of width of second set of sheath flow channels

Figure 6 presents the numerical results obtained for the cross-sectional distribution of the sample stream in the micro-weir region of cytometers in which the second set of sheath flow channels have different widths. Note that the horizontal focusing ratio is assumed to be 4:1 in every case, while the entrance angle and depth of the second set of sheath flow channels are specified as 90° and 26 μm , respectively. Here, the width ratio (d/D) is defined as: (the width of the second set of sheath flow channels d /the width

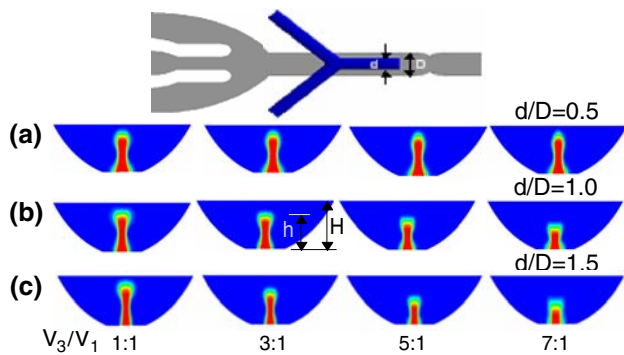


Fig. 6 Simulation results obtained for sample stream distribution in micro-weir region for a constant horizontal focusing ratio of 4:1, different vertical focusing ratios, a constant secondary sheath flow angle of 90° and width ratios of: **a** 0.5, **b** 1.0 and **c** 1.5

of the main channel D). The results show that for a width ratio of 0.5, the relative focused height of the sample stream is insensitive to the value of the vertical focusing ratio. However, for width ratios of 1.0 and 1.5, respectively, a notable reduction in the sample height is observed at values of the vertical focusing ratio greater than 3:1.

Figure 7 illustrates the variation of the relative height of the focused sample stream with the vertical focusing ratio as a function of the width ratio. Note that the horizontal focusing ratio is assumed to be 4:1 and the entrance angle of the second set of sheath flow channels is 90° . The results reveal that when the ratio of the sheath flow channel width to the main channel width is assigned a small value, i.e. $d/D = 0.5$, the sample height can not be reduced by more

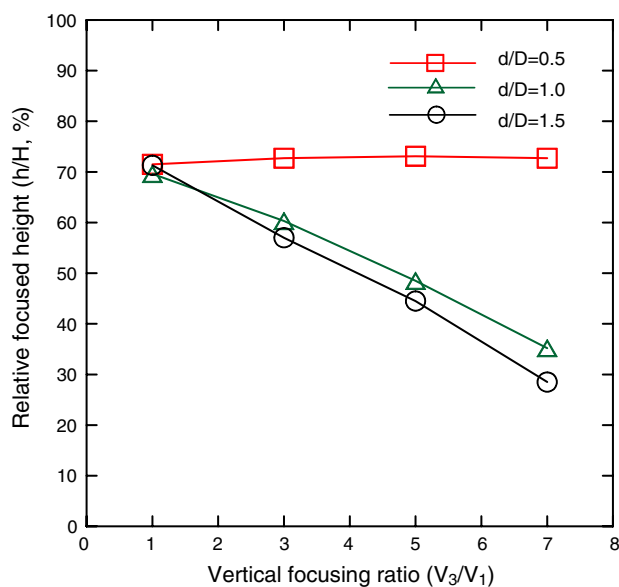


Fig. 7 Variation of relative focused height of sample stream in micro-weir region with vertical focusing ratio as function of width ratio. (Note that the results are obtained using a constant horizontal focusing ratio of 4:1.)

than 30% of its original value, even at the highest vertical focusing ratio of 7:1. The numerical experiments show that the total momentum of the second sheath flow is too low to displace the sample stream in the center. Most second sheath flow merges with the first sheath flow, and diminishes the hydrodynamic focusing effect on the sample flow. However, when the width ratio is increased to 1.0 or 1.5, respectively, the relative focused height of the sample stream reduces steadily from an initial value of 70% (at a vertical focusing ratio of 1.0) to a final value of approximately 35 or 30%, respectively, at a vertical focusing ratio of 7:1. In general, the fabrication procedure is simplified when the microchannels within the cytometer have the same dimensions. Thus, Fig. 7 indicates that a width ratio of 1:0 represents the optimal design solution for the second set of sheath flow channels.

3.4 Effect of depth of second set of sheath flow channels

Figure 8 presents the numerical results obtained for the cross-sectional distribution of the sample stream in the micro-weir region of the microchannel in cytometers in which the second set of sheath flow channels have different depths. As before, a constant horizontal focusing ratio of 4:1 is assumed, while the entrance angle and width ratio of the second set of sheath flow channels are specified as 90° and 1:1, respectively. Here, the depth ratio (W_2/W_1) is defined as: [the depth of the second set of sheath flow channels W_2 /the depth of the main channel W_1]. Figure 8a shows that for a depth ratio of 0.5, there is virtually no

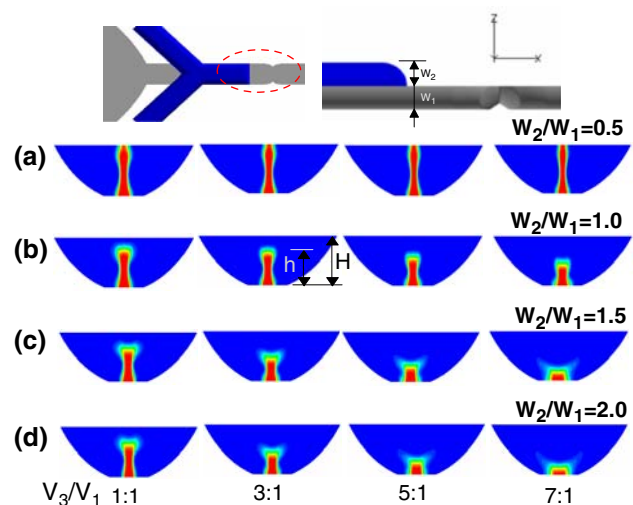


Fig. 8 Simulation results obtained for sample stream distribution in micro-weir region for a constant horizontal focusing ratio of 4:1, different vertical focusing ratios, a constant secondary sheath flow angle of 90° , a constant width ratio of 1:1 and depth ratios of: **a** 0.5, **b** 1.0, **c** 1.5 and **d** 2.0

change in the cross-sectional distribution of the sample stream as the vertical focusing ratio is increased. However, Fig. 8b shows that when the depth ratio is increased to 1.0, a notable reduction in the sample height is obtained at values of the vertical focusing ratio greater than 5:1. When the depth ratio is increased to 1.5 or 2.0, respectively, it can be seen that a further reduction in the sample height is obtained (see Fig. 8c, d), with both sheath flows reducing the sample height to around 40% of its original value at a vertical focusing ratio of 3:1.

Figure 9 illustrates the variation of the relative focused height of the sample stream with the vertical focusing ratio as a function of the depth ratio. Note that in computing the results, the horizontal focusing ratio is assigned a constant value of 4:1, the width ratio is 1:1 and the entrance angle of the second set of sheath flow channels is 90°. At the lowest depth ratio of 0.5, it can be seen that the sample retains its original height irrespective of the value of the vertical focusing ratio. The main reason is that the momentum of the second sheath flow is too low to displace the sample stream in the center. However, when the depth ratio is increased to 1.0, the relative focused height reduces from around 70–35% as the vertical focusing ratio is increased from 1:1 to 7:1. When the depth ratio is further increased to 1.5 or 2.0, respectively, a significant reduction in the sample height is achieved, with relative focused heights of around 12 and 8%, respectively, at the maximum vertical focusing ratio of 7:1. Overall, the results presented in Fig. 9 indicate that a depth ratio of 1.5 represents the optimal design for the second set of sheath flow channels.

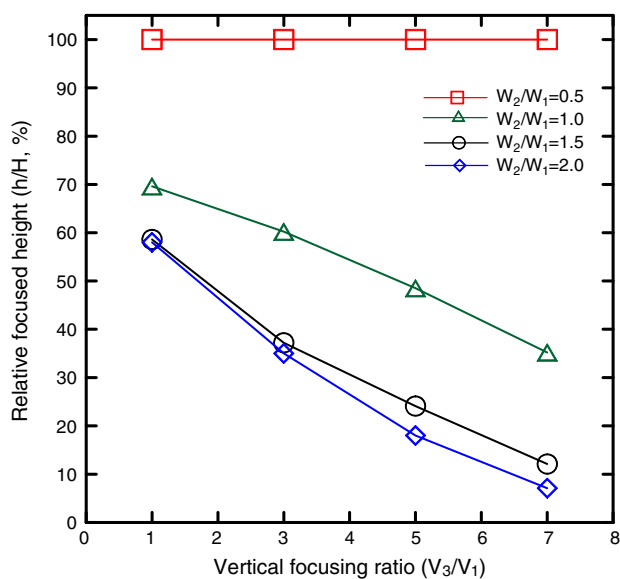


Fig. 9 Variation of relative focused height of sample stream in micro-weir region with vertical focusing ratio as function of depth ratio. (Note that the results are obtained using a constant horizontal focusing ratio of 4:1.)

3.5 Effect of micro-weir structure

In this section, we demonstrate the important role that the weir plays. The characteristic of weir are independent of the vertical focusing ratios, and the weir can function well at various vertical focusing ratios. Therefore, the case of the vertical focusing ratio 3:1 is conducted to elucidate the weir function. Figure 10 presents the streamline distributions in the micro-flow cytometer with the geometrical parameters, i.e. an entrance angle of the second set of sheath flow channels of 90°, a width ratio of 1.0 and a depth ratio of 1.5. Note that in performing the simulations, the horizontal focusing ratio is specified as 4:1, while the vertical focusing ratio is assumed to be 3:1. In general, the results indicate that these geometry and operational parameter settings cause the sample stream to be located centrally in both the horizontal X-Y plane and the vertical X-Z plane.

Figure 11 presents the numerical results obtained for the cross-sectional distribution of the sample stream at various positions of the microchannel under a horizontal focusing ratio of 4:1 and a vertical focusing ratio of 3:1. Figure 11a and b show that prior to the outlets of the second set of sheath flow channels, the width and height of the sample stream remain relatively unchanged as it travels along the microchannel since it is constrained only by the horizontal focusing effect. However, as the sample passes the outlets of the second set of sheath flow channels and travels toward the micro-weir structure, both the width and the height of the sample stream decrease (see Fig. 11c–f).

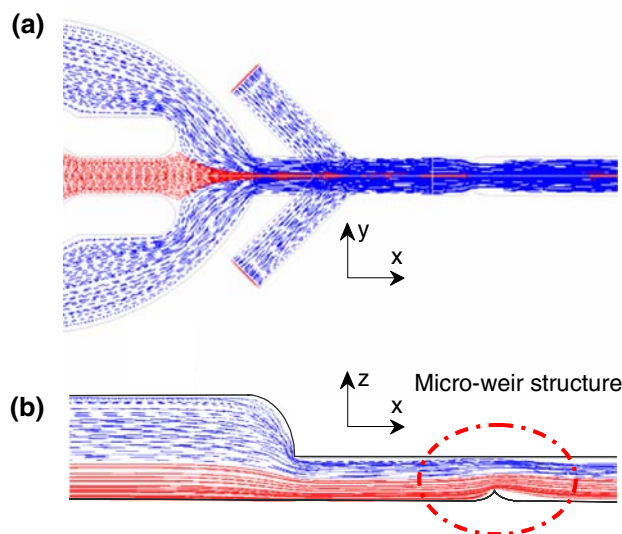


Fig. 10 Streamline distributions in micro-flow cytometer for a constant horizontal focusing ratio of 4:1 and a constant vertical focusing ratio of 3:1: **a** top view and **b** side view

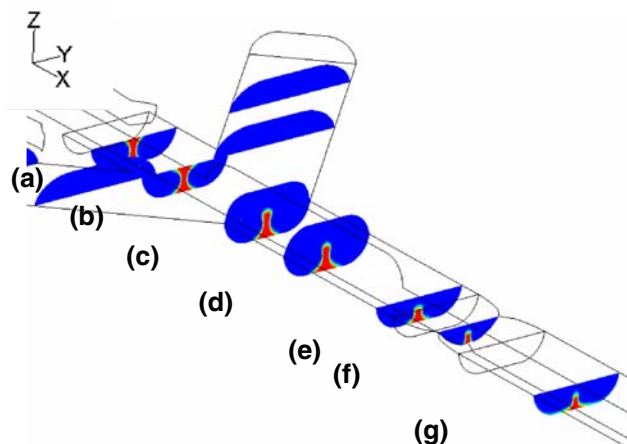


Fig. 11 Simulation results for sample stream profile at various cross-sections for horizontal focusing ratio of 4:1 and vertical focusing ratio of 3:1

Downstream of the micro-weir structure, however, the sample is restored to its original width, although a slight diffusion effect is observed (see Fig. 11g).

To fully clarify the effect of the micro-weir structure on the flow pattern within the cytometer, the Crank-Nicolson method (Yang and Fu 2001; Fu et al. 2004b) was used to predict the traces of two representative micro-particles within the fluid in accordance with the velocity field ($dx/dt = u$). In the analysis, it was assumed that the two micro-particles were injected simultaneously into the microchannel at different heights (i.e. different Z-axis locations), but at the same cross-section (i.e. the same X-axis location). The trajectories of the two particles were then simulated over time as they flowed in the downstream direction past the micro-weir structure. At time $t + \Delta t$, each micro-particle moves a distance $\Delta t \times u$, where u is the velocity and is obtained via a process of linear interpolation between the surrounding grid points. The new micro-particle velocity at time t is obtained in a similar manner and the velocity of the micro-particle over time Δt is then obtained by time-averaging the two velocity values.

Figure 12a and b present the simulated traces of the two particles in the X-Y and X-Z planes, respectively, over six sequential time-steps. Note that the cytometer is assumed to have the optimal geometrical configuration and the horizontal and vertical focusing ratios are specified as 4:1 and 3:1, respectively. As shown, at time $t = 1$, the two particles are located in the center of the focused sample stream in the X-Y plane, but are positioned vertically one on top of the other in the X-Z plane such that only the upper particle is visible. However, as the particles pass the outlets of the second set of sheath flow channels and approach the micro-weir region (i.e. time-steps $t = 2$ to 5), they remain

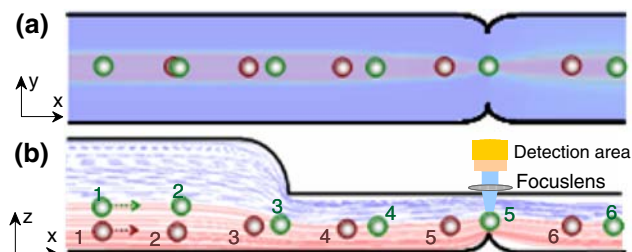


Fig. 12 Numerical trace results for micro-particle distributions in: a X-Y and b X-Z planes

focused in the center of the microchannel in the X-Y plane, but are gradually separated in the X-Z plane such that they flow through the detection area sequentially. Following their passage through the micro-weir region, the two particles retain their spacing in the X-Z plane and remain focused in the center of the microchannel in both the horizontal and the vertical planes (see $t = 6$).

4 Conclusions

This study has presented a novel 3-D focusing micro-flow cytometer featuring two pairs of hydrodynamic sheath flows and a micro-weir structure. In the proposed approach, the sample stream is focused initially in the horizontal plane using two sheath flows and is then focused in the vertical direction using a second set of sheath flows and a micro-weir structure. The performance of the proposed device has been characterized via a series of CFD numerical simulations and the optimal cytometer geometry parameters and focusing ratios have been established. The numerical results have shown that the proposed 3-D focusing approach not only confines the cells/particles to the central region of the microchannel in the horizontal plane, but also separates them in the vertical plane such that they flow through the detection region on a one-by-one basis. As a result, the cytometer enables a more reliable detection and counting operation than conventional 2-D focusing micro-cytometers in which the cells/particles may be overlapped in the vertical direction or may be distributed non-uniformly in the vertical plane, thus limiting the effectiveness of the detection system. It has been shown that the proposed 3-D focusing system is capable of compressing the sample stream width to the order of $6 \sim 15 \mu\text{m}$ via an appropriate specification of the horizontal focusing ratio. Consequently, it can be inferred that the micro-flow cytometer represents an ideal solution for cell and particle counting applications in the microfluidics and clinical domains.

Acknowledgments The current authors gratefully acknowledge the financial support provided to this study by the National Science Council of Taiwan under Grant NSC95-2314-B-020-001-MY2.

References

- Bown MR, Meinhart CD (2006) AC electroosmotic flow in a DNA concentrator. *Microfluid Nanofluid* 2:513–523
- Chang CC, Yang RJ (2007) Electrokinetic mixing in microfluidic systems. *Microfluid Nanofluid* 3:501–525
- Chang YH, Lee GB, Huang FC, Chen YY, Lin JL (2006) Integrated polymerase chain reaction chips utilizing digital microfluidics. *Biomed Microdevices* 8:215–225
- Chang CC, Huang ZX, Yang RJ (2007) Three-dimensional hydrodynamic focusing in two-layer polydimethylsiloxane (PDMS) microchannels. *J Micromech Microeng* 17:1479–1486
- Chen D, Du H (2007) A dielectrophoretic barrier-based microsystem for separation of microparticles. *Microfluid Nanofluid* 3:603–610
- Cheng IF, Chang HC, Hou D, Chang HC (2007) An integrated dielectrophoretic chip for continuous bioparticle filtering, focusing, sorting, trapping, and detecting. *Biomicrofluidics* 1:021503
- Dittrich PS, Schuille P (2003) An integrated microfluidic system for reaction, high-sensitivity detection, and sorting of fluorescent cells and particles. *Anal Chem* 75:5767–5774
- Emmelkamp J, Wolbers F, Andersson H, DaCosta RS, Wilson BC, Vermes I, van den Berg A (2004) The potential of autofluorescence for the detection of single living cells for label-free cell sorting in microfluidic systems. *Electrophoresis* 25:3740–3745
- Erickson D (2005) Towards numerical prototyping of labs-on-chip: modeling for integrated microfluidic devices. *Microfluid Nanofluid* 1:301–318
- Fu LM, Lin CH (2007) A rapid DNA digestion system. *Biomed Microdevices* 9:277–286
- Fu LM, Yang RJ, Lee GB, Pan YJ (2003) Multiple injection techniques for microfluidic sample handling. *Electrophoresis* 24:3026–3032
- Fu LM, Lee GB, Lin YH, Yang RJ (2004a) Manipulation of microparticles using new modes of travelling-wave-dielectrophoretic forces: numerical simulation and experiments. *IEEE ASME Trans Mechatron* 9:377–383
- Fu LM, Yang RJ, Lin CH, Pan YJ, Lee GB (2004b) Electrokinetically driven micro flow cytometers with integrated fiber optics for on-line cell/particle detection. *Anal Chim Acta* 507:163–169
- Fu LM, Tsai CH, Lin C H (2008) A high-discernment micro-flow cytometer with micro-weir structure. *Electrophoresis* (in press)
- Hardt S, Schonfeld F (2003) Laminar mixing in different interdigital micromixers: II. numerical simulations. *AIChE J* 49:578–584
- Holmes D, Morgan H, Green NG (2006) High throughput particle analysis: combining dielectrophoretic particle focusing with confocal optical detection. *Biosens Bioelectron* 21:1621–1630
- Huang MZ, Yang RJ, Tai CH, Tsai CH, Fu LM (2006) Application of electrokinetic instability flow for enhanced micromixing in cross-shaped microchannel. *Biomed Microdevices* 8:309–315
- Hunt HC, Wilkinson JS (2008) Optofluidic integration for microanalysis. *Microfluid Nanofluid* 4:53–59
- Kohlheyer D, Unnikrishnan S, Besselink GAJ, Schlautmann S, Schasfoort RBM (2008) A microfluidic device for array patterning by perpendicular electrokinetic focusing. *Microfluid Nanofluid* (in press)
- Lacharme F, Gijjs MAM (2006) Single potential electrophoresis microchip with reduced bias using pressure pulse injection. *Electrophoresis* 27:2924–2932
- Lee GB, Hung CI, Ke BJ, Huang GR, Hwei BH, Lai HF (2001) Hydrodynamic focusing for a micromachined flow cytometer. *Trans ASME* 123:672–679
- Lee GB, Lin CH, Chang GL (2003) Micro flow cytometers with buried SU-8/SOG optical waveguides. *Sensors Actuator A* 103:165–170
- Lee GB, Chang CC, Huang SB, Yang RJ (2006) The hydrodynamic focusing effect inside rectangular microchannels. *J Micromech Microeng* 16:1024–1032
- Lee CY, Chen CM, Chang GL, Lin CH, Fu LM (2006) Fabrication and characterization of semicircular detection electrodes for contactless conductivity detector—capillary electrophoresis microchips. *Electrophoresis* 27:5043–5050
- Lin CH, Lee GB, Fu LM, Chen SH (2004a) Integrated optical-fiber capillary electrophoresis microchips with novel spin-on-glass surface modification. *Biosens Bioelectron* 20:83–90
- Lin CH, Lee GB, Fu LM, Hwei BH (2004b) Vertical focusing device utilizing dielectrophoretic force and its application on microflow cytometer. *J Microelectromech Syst* 13:923–932
- Mao X, Waldeisen JR, Huang TJ (2007) “Microfluidic drifting”—implementing three-dimensional hydrodynamic focusing with a single-layer planar microfluidic device. *Lab Chip* 7:1260–1262
- McClain MA, Culbertson CT, Jacobson SC, Ramsey JM (2001) Flow cytometry of *Escherichia coli* on microfluidic devices. *Anal Chem* 73:5334–5338
- McClain MA, Culbertson CT, Jacobson SC, Allbritton NL, Sims CE, Ramsey JM (2003) Microfluidic devices for the high-throughput chemical analysis of cells. *Anal Chem* 75:5646–5655
- Prakash R, Kaler KVIS (2007) An integrated genetic analysis microfluidic platform with valves and a PCR chip reusability method to avoid contamination. *Microfluid Nanofluid* 3:177–181
- Rodriguez-Trujillo R, Mills CA, Samitier J, Gomila G (2007) Low cost micro-Coulter counter with hydrodynamic focusing. *Microfluid Nanofluid* 3:171–176
- Stiles T, Fallon R, Vestad T, Oakey J, Marr DWM, Squier J, Jimenez R (2005) Hydrodynamic focusing for vacuum-pumped microfluidics. *Microfluid Nanofluid* 1:280–283
- Sundararajan N, Pio MS, Lee LP, Berlin AA (2004) Three-dimensional hydrodynamic focusing in polydimethylsiloxane (PDMS) microchannels. *J Microelectromech Syst* 13:559–67
- Tsai CH, Yang RJ, Tai CH, Fu LM (2005) Numerical simulation of electrokinetic injection techniques in capillary electrophoresis microchips. *Electrophoresis* 26:674–686
- Tsai CH, Chen HT, Wang YN, Lin CH, Fu LM (2007) Capabilities and limitations of 2-dimensional and 3-dimensional numerical methods in modeling the fluid flow in sudden expansion microchannels. *Microfluid Nanofluid* 3:13–18
- Tůma P, Samcová E, Opekar F, Jurka V, Štulík K (2007) Determination of 1-methylhistidine and 3-methylhistidine by capillary and chip electrophoresis with contactless conductivity detection. *Electrophoresis* 28:2174–2180
- Van Doormal JP, Raithby GD (1984) Enhancements of the SIMPLE method for predicting incompressible fluid flows. *Numer Heat Transfer* 7:147–163
- Wang Z, Hansen O, Petersen PK, Rogeberg A, Kutter JP, Bang DD, Wolff A (2006) Dielectrophoresis microsystem with integrated flow cytometers for on-line monitoring of sorting efficiency. *Electrophoresis* 27:5081–5092
- Wolff A, Perch-Nielsen IR, Larsen UD, Friis P, Goranovic G, Poulsen CR, Kutter JP, Telleman P (2003) Integrating advanced functionality in a microfabricated high-throughput fluorescent activated cell sorter. *Lab Chip* 3(1):22–27

- Wu Z, Liu AO, Hjort K (2007) Microfluidic continuous particle/cell separation via electroosmotic-flow-tuned hydrodynamic spreading. *J Micromech Microeng* 17:1992–1999
- Xia N, Hunt TP, Mayers BT, Alsberg E, Whitesides GM, Westervelt RM, Ingber DE (2006) Combined microfluidic-micromagnetic separation of living cells in continuous flow. *Biomed Microdevices* 8:299–308
- Xuan X, Li D (2005) Focused electrophoretic motion and selected electrokinetic dispensing of particles and cells in cross-microchannels. *Electrophoresis* 26:3552–3560
- Yang RJ, Fu LM (2001) Thermal and flow analysis of a heated electronic component. *Int J Heat Mass Transfer* 44:2261–2275
- Yang AS, Hsieh WH (2007) Hydrodynamic focusing investigation in a micro-flow cytometer. *Biomed Microdevices* 9:113–122
- Yang R, Feedback DL, Wang W (2005) Microfabrication and test of a three-dimensional polymer hydro-focusing unit for flow cytometry applications. *Sens Actuators A* 118:259–267
- Yu C, Vykoukal J, Vykoukal DM, Schwartz JA, Shi L, Gascoyne PRC (2005) A three-dimensional dielectrophoretic particle focusing channel for microcytometry application. *J Microelectromech Syst* 14:480–487
- Zhuang GS, Li G, Jin QH, Zhao JL, Yang MS (2006) Numerical analysis of an electrokinetic double-focusing injection technique for microchip CE. *Electrophoresis* 27:5009–5019
- Zou H, Mellon S, Syms RRA, Tanner KE (2006) 2-dimensional MEMS dielectrophoresis device for osteoblast cell stimulation. *Biomed Microdevices* 8:353–359